





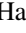



Lindblad dynamics from spatio-temporal correlation functions in nonintegrable spin-1/2 chains with different boundary conditions

Markus Kraft ^{1,*}, Jonas Richter ^{2,3}, Fengping Jin ⁴, Sourav Nandy ⁵, Jacek Herbrych ⁶, Kristel Michielsen ⁴,
Hans De Raedt ⁷, Jochen Gemmer,¹ and Robin Steinigeweg ^{1,†}

¹Department of Mathematics/Computer Science/Physics, *University of Osnabrück*, D-49076 Osnabrück, Germany

²Department of Physics, *Stanford University*, Stanford, California 94305, USA

³Institut für Theoretische Physik, *Leibniz Universität Hannover*, 30167 Hannover, Germany

⁴Institute for Advanced Simulation, *Jülich Supercomputing Centre, Forschungszentrum Jülich*, D-52425 Jülich, Germany

⁵Jožef Stefan Institute, 1000 Ljubljana, Slovenia

⁶Institute of Theoretical Physics, Faculty of Fundamental Problems of Technology, *Wrocław University of Science and Technology*, 50-370 Wrocław, Poland

⁷Zernike Institute for Advanced Materials, *University of Groningen*, 9747 AG Groningen, Netherlands



(Received 8 March 2024; accepted 15 May 2024; published 6 June 2024)

We investigate the Lindblad equation in the context of boundary-driven magnetization transport in spin-1/2 chains. Our central question is whether the nonequilibrium steady state of the open system, including its buildup in time, can be described on the basis of the dynamics in the closed system. To this end, we rely on a previous study [Heitmann *et al.*, *Phys. Rev. B* **108**, L201119 (2023)], in which a description in terms of spatio-temporal correlation functions was suggested in the case of weak driving and small system-bath coupling. Because this work focused on integrable systems and periodic boundary conditions, we here extend the analysis in three directions: (1) We consider nonintegrable systems, (2) we take into account open boundary conditions and other bath-coupling geometries, and (3) we provide a comparison to time-evolving block decimation. While we find that nonintegrability plays a minor role, the choice of the specific boundary conditions can be crucial due to potentially nondecaying edge modes. Our large-scale numerical simulations suggest that a description based on closed-system correlation functions is a useful alternative to already existing state-of-the-art approaches.

DOI: [10.1103/PhysRevResearch.6.023251](https://doi.org/10.1103/PhysRevResearch.6.023251)

I. INTRODUCTION

Quantum many-body systems out of equilibrium are a central topic of modern physics, and they have attracted increasing attention over recent years, both experimentally and theoretically [1–5]. Key questions in this context are the emergence and properties of steady states in the limit of long times and also the actual route to such states in the course of time [2–5]. The understanding of these questions is of importance to isolated systems without any coupling to an environment and open systems with weak or strong coupling to a bath, and it has witnessed rather remarkable progress due to fresh concepts like eigenstate thermalization [6–8] and the typicality of random pure states [9–17] and due to the development of sophisticated numerical techniques [18,19].

In systems with a globally conserved quantity, a quite natural nonequilibrium process is given by transport [20]. It

is a prime example of relevance to closed and open systems alike, in addition to the relevance of steady states and the relaxation to them. In isolated systems, a widely used approach is linear-response theory, which yields the well-known Kubo formula in terms of current autocorrelation functions [21]. This theory can be formulated for density-density correlation functions as well, either in momentum and frequency space or in the space and time domain. While linear response provides a clear-cut strategy, the concrete evaluation of correlation functions for specific models has turned out to be an analytical and numerical challenge, even for seemingly simple models of the Heisenberg or Hubbard type in one dimension [20], with the most recent progress being by generalized hydrodynamics [22,23].

In an open-system scenario, transport can be induced by coupling the system to baths at different temperatures or chemical potentials, which then usually yields a nonequilibrium steady state with a constant current and characteristic density profile in the long-time limit [24–27]. Such a scenario is often modeled by an equation of Lindblad form [28]. While the derivation of this equation from a microscopic system-bath model is a nontrivial task in practice [26,29], it is the most general version of a time-local master equation, which maps any density matrix to another density matrix. In particular, it allows for efficient numerical treatment by matrix-product states for quite large system sizes [24,30–32], as dissipation

*markus.kraft@uos.de

†rsteinig@uos.de

Published by the American Physical Society under the terms of the [Creative Commons Attribution 4.0 International](https://creativecommons.org/licenses/by/4.0/) license. Further distribution of this work must maintain attribution to the author(s) and the published article's title, journal citation, and DOI.

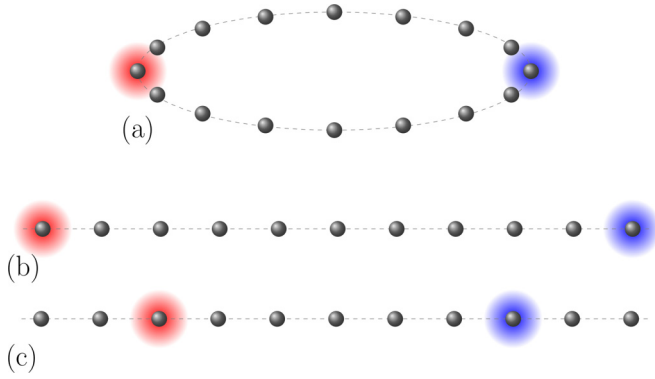


FIG. 1. Sketch of the three different geometries of the bath coupling. (a) Periodic boundary conditions. (b) and (c) Open boundary conditions with the bath coupling located exactly at the edges or close to the edges of the system. Note that open boundary conditions should not be confused with the open-system scenario.

reduces the unavoidable growth of entanglement as a function of time.

The two complementary approaches of closed and open systems have been the basis for reliable identification of different dynamical phases, including the case of normal diffusion [20], and also for other transport [33–44] types ranging from ballistic to anomalous dynamics. Moreover, quantitative agreement of diffusion constants was found in some cases [45–48]. However, clear correspondence between the dynamics in closed and open systems is still lacking [49–51]. Thus, the main question of the present paper is, Can one predict the open-system dynamics based on knowledge of the closed-system time evolution? While a general answer to this question appears to be hopeless, it might be possible for specific models and parameters at least.

To investigate this question, we rely here on a previous study [52], in which spatio-temporal correlation functions were suggested as a convenient ingredient in the case of weak driving and small system-bath coupling. Because the aforementioned work focused on integrable systems and periodic boundary conditions, we intend to extend the analysis in three different directions: (1) We consider nonintegrable systems, (2) we take into account open boundary conditions and other bath-coupling geometries (see Fig. 1), and (3) we provide a comparison to time-evolving block decimation (TEBD). While we find that nonintegrability plays a minor role, the choice of the specific boundary conditions can be crucial due to potentially nondecaying edge modes. Our large-scale numerical simulations suggest that a description based on closed-system correlation functions constitutes a useful alternative to existing state-of-the-art approaches.

Our paper is organized as follows. To begin with, we introduce in Sec. II the closed-system models studied here and the spatio-temporal correlation functions. Then, in Sec. III, we discuss the concept of dynamical quantum typicality and describe its implications for numerical and analytical purposes. Afterwards, in Sec. IV, we continue with the open-system setup, and then we review the technique of stochastic unraveling in Sec. V. Section VI is devoted to the central prediction used later and its underlying assumptions. Next, in Sec. VII,

we present our results. We conclude in Sec. VIII and give additional information in the Appendixes.

II. CLOSED MODELS AND SPATIO-TEMPORAL CORRELATION FUNCTIONS

In this paper, we consider two different paradigmatic examples of quantum many-body models which have previously attracted significant attention in the literature on, e.g., transport. These two examples are nonintegrable modifications of the integrable spin-1/2 XXZ model in one dimension. The Hamiltonian of this model is given by [20]

$$H_{\text{obc}} = J \sum_{r=1}^{N-1} (S_r^x S_{r+1}^x + S_r^y S_{r+1}^y + \Delta S_r^z S_{r+1}^z), \quad (1)$$

where S_r^i ($i = x, y, z$) are spin-1/2 operators at site r , N is the total number sites, $J > 0$ is the antiferromagnetic exchange coupling constant, and Δ is the anisotropy in the z direction. While the Hamiltonian in Eq. (1) is denoted for open boundary conditions, we will also use periodic boundary conditions,

$$H_{\text{pbc}} = H_{\text{obc}} + J(S_N^x S_1^x + S_N^y S_1^y + \Delta S_N^z S_1^z), \quad (2)$$

where the numbers of sites N is chosen to be even. The specific choice of boundary conditions will play an important role in the open setup, which will be discussed later in detail.

The spin-1/2 XXZ chain is well known to be integrable for any value of Δ , and it was the focus of our previous work [52]. In this work, we go beyond it and include integrability-breaking perturbations, which then yield a more generic situation. As the first type of perturbation, we choose further interactions between next-nearest sites, which lead, for open boundary conditions, to

$$H'_{\text{obc}} = H_{\text{obc}} + J\Delta' \sum_{r=1}^{N-2} S_r^z S_{r+2}^z \quad (3)$$

and, although not shown explicitly, to a corresponding form for periodic boundary conditions. Here, Δ' is the strength of the perturbation, and we will focus on the particular value $\Delta' = 0.5$, for which integrability is well broken. As the second type of perturbation, we choose a Zeeman term with a staggered magnetic field,

$$H''_{\text{obc/pbc}} = H_{\text{obc/pbc}} + B \sum_{r=1}^N (-1)^r S_r^z, \quad (4)$$

where we set the strength of the perturbation to the specific value $B/J = 0.5$ for the same reason as above.

Since the total magnetization $S^z = \sum_r S_r^z$ is strictly conserved for the models in Eqs. (3) and (4), $[H, S^z] = 0$, transport of spins is a meaningful question. Within the different approaches to transport in general, linear-response theory is one of the main concepts. While this theory leads to the Kubo formula and current autocorrelation functions [21], it is also the basis for spatio-temporal correlation functions,

$$\langle S_r^z(t) S_r^z(0) \rangle_{\text{eq}} = \frac{\text{tr}[e^{-\beta H} e^{iHt} S_r^z e^{-iHt} S_r^z]}{\text{tr}[e^{-\beta H}]}. \quad (5)$$

Here, $\beta = 1/T$ is the inverse temperature (measured in units of the Boltzmann constant), and from now on we will

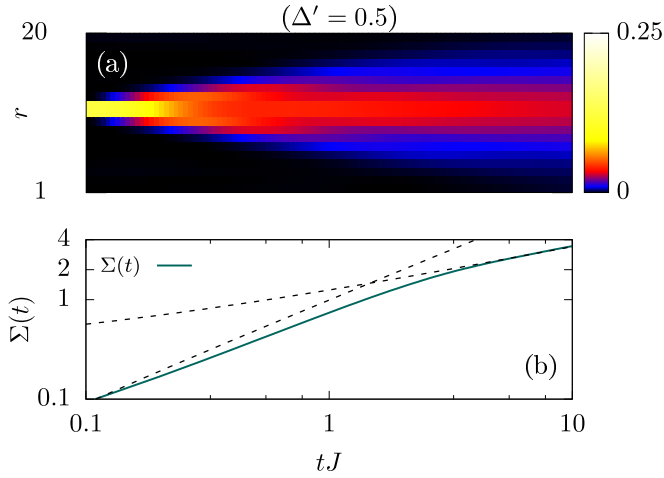


FIG. 2. (a) Time-space density plot of the correlation function $\langle S_r^z(t) S_{r'}^z(0) \rangle_{\text{eq}}$, as obtained numerically for the Hamiltonian H' in Eq. (3) with $\Delta = 1.5$, $\Delta' = 0.5$, $N = 20$, $r' = N/2 + 1 = 11$, and periodic boundary conditions. (b) Corresponding time evolution of the standard deviation $\Sigma(t)$ as well as two power laws, $\propto t^1$ and $\propto t^{1/2}$, in a double-logarithmic plot.

consider the high-temperature limit $\beta \rightarrow 0$, which still features nontrivial transport properties. The correlation functions in Eq. (5) measure the overlap of a time-evolved $S_r^z(t)$ at some site r with an initial $S_{r'}^z(0)$ at another site r' . In Fig. 2(a), we illustrate the space-time dependence, as obtained numerically for the Hamiltonian H' in Eq. (3) with $\Delta = 1.5$, $\Delta' = 0.5$, $N = 20$, and periodic boundary conditions. Initially, there is a δ -function peak at the site $r = r'$ and a uniform equilibrium background at other sites $r \neq r'$. The subsequent broadening of the δ -function peak corresponds to transport.

A convenient way to analyze the type of transport is provided by the spatial variance [53]

$$\Sigma^2(t) = \sum_r (r - r')^2 C_{rr'}(t) - \left[\sum_r (r - r') C_{rr'}(t) \right]^2, \quad (6)$$

where the distribution $C_{rr'}(t) = 4 \langle S_r^z(t) S_{r'}^z(0) \rangle_{\text{eq}}$ is a normalized version of Eq. (5), $\sum_r C_{rr'}(t) = 1$. For diffusive transport, $\Sigma(t) \propto t^{1/2}$. In Fig. 2(b), we depict $\Sigma(t)$ for the example in Fig. 2(a). While it is clear that a ballistic growth $\Sigma(t) \propto t$ has to take place at short times, there is a diffusive growth $\Sigma(t) \propto t^{1/2}$ at intermediate times, as expected due to the non-integrability of the model [54]. It is worth mentioning that the integrable model in Eq. (1) features a richer phase diagram, including superdiffusive behavior for $\Delta = 1$ and ballistic behavior for $\Delta < 1$. The different types of transport become manifest in the quantity [53]

$$D(t) = \frac{1}{2} \frac{d}{dt} \Sigma^2(t), \quad (7)$$

which becomes constant in the case of diffusion.

Let us mention here that the spatio-temporal correlation function $\langle S_r^z(t) S_{r'}^z(0) \rangle_{\text{eq}}$ not only is a strategy to study transport in closed systems but may also be used to predict the buildup of a nonequilibrium steady state in open systems, where a bath is coupled at each edge. Investigating the quality of such a prediction is a central point of our paper. However, before

we discuss this point in detail, we need to introduce further concepts.

III. DYNAMICAL QUANTUM TYPICALITY

Next, let us discuss dynamical quantum typicality as one of the central concepts applied in this paper. On the one hand, this concept provides the basis for a numerical calculation of the spatio-temporal correlation functions $\langle S_r^z(t) S_{r'}^z(0) \rangle_{\text{eq}}$ in closed systems of comparatively large size. On the other hand, it constitutes a main ingredient to connect these correlation functions to the dynamics in open systems, as we will see later.

Loosely speaking, the basic idea of typicality is that a single pure state can imitate the full statistical ensemble on the level of the corresponding expectation values [9–13]. To be precise, we introduce a pure state drawn at random (according to the Haar measure) from a Hilbert space of high dimension D ,

$$|\psi\rangle = \sum_{n=1}^D c_j |j\rangle, \quad (8)$$

where $\{|j\rangle\}$ is an arbitrary orthonormal basis and the real and imaginary parts of the coefficients $c_j = a_j + ib_j$ result from a Gaussian probability distribution with zero mean and unit variance. For such a pure state, we then obtain the approximation [16,17]

$$\langle S_r^z(t) S_{r'}^z(0) \rangle_{\text{eq}} = \frac{\langle \psi | S_r^z(t) S_{r'}^z(0) | \psi \rangle}{\langle \psi | \psi \rangle} + O\left(\frac{1}{\sqrt{D}}\right), \quad (9)$$

where the statistical error on the right-hand side is exponentially small in system size because $D = 2^N$. This approximation can be rewritten as

$$\langle S_r^z(t) S_{r'}^z(0) \rangle_{\text{eq}} \approx \frac{\langle \psi(t) | S_r^z | \phi(t) \rangle}{\langle \psi | \psi \rangle}, \quad (10)$$

using the two auxiliary pure states $|\psi(t)\rangle = e^{-iHt} |\psi\rangle$ and $|\phi(t)\rangle = e^{-iHt} S_{r'}^z |\psi\rangle$. Expression (10), just like analogous expressions for other observables, has turned out to be particularly useful for numerical simulations since its evaluation requires forward propagation of pure states in time. These propagations can be carried out efficiently in huge Hilbert spaces, which are orders of magnitude larger than the ones accessible by standard exact diagonalization [16,17]. Note that the numerical data in Fig. 2 are also obtained in this way, but on the basis of a slightly different and simpler expression, as explained in the following.

The simplification employs the fact that S_r^z and $n_r = S_r^z + 1/2$ are operators with the specific properties $\text{tr}[S_r^z] = 0$ and $n_r^2 = n_r$. Using these two properties and introducing the pure state

$$|\varphi(t)\rangle = e^{-iHt} n_{r'} |\psi\rangle \quad (11)$$

then lead to the expression [55]

$$\langle S_r^z(t) S_{r'}^z(0) \rangle_{\text{eq}} \approx \frac{1}{2} \frac{\langle \varphi(t) | S_r^z | \varphi(t) \rangle}{\langle \varphi | \varphi \rangle}, \quad (12)$$

which involves only a single pure state. This expression has an obvious numerical benefit but also provides a central analytical relation for later purposes in the context of open systems.

IV. OPEN SETUP AND LINDBLAD EQUATION

Now, let us turn to an open-system scenario, where we couple the system to an environment. We describe this scenario using the Lindblad equation,

$$\dot{\rho}(t) = \mathcal{L}\rho(t) = i[\rho(t), H] + \mathcal{D}\rho(t), \quad (13)$$

as the most general form of a time-local quantum master equation which maps any density matrix to another density matrix [28]. The Lindblad equation (13) consists of a coherent part for the unitary time evolution with respect to H and an incoherent damping term. This damping term is given by

$$\mathcal{D}\rho(t) = \sum_j \alpha_j \left(L_j \rho(t) L_j^\dagger - \frac{1}{2} \{ \rho(t), L_j^\dagger L_j \} \right), \quad (14)$$

with non-negative rates α_j , Lindblad operators L_j , and the anticommutator $\{\bullet, \bullet\}$. Despite the generality of the Lindblad equation, its derivation is a challenging task for a specific microscopic model [26,29].

Here, we couple our system to two baths and choose the respective Lindblad operators [20]

$$L_1 = S_{B_1}^+, \quad \alpha_1 = \gamma(1 + \mu), \quad (15)$$

$$L_2 = L_1^\dagger = S_{B_1}^-, \quad \alpha_2 = \gamma(1 - \mu), \quad (16)$$

$$L_3 = S_{B_2}^+, \quad \alpha_3 = \gamma(1 - \mu), \quad (17)$$

$$L_4 = L_3^\dagger = S_{B_2}^-, \quad \alpha_4 = \gamma(1 + \mu), \quad (18)$$

where γ is the system-bath coupling and μ is the driving strength. L_1 and L_2 are local operators, which act on a site B_1 and flip a spin up and down, respectively. L_3 and L_4 are corresponding operators at another site B_2 .

Our different choices of the bath-contact sites B_1 and B_2 are illustrated in Fig. 1. In the case of periodic boundary conditions, we set $B_1 = 1$ and $B_2 = N/2 + 1$ at a distance $N/2$ [see Fig. 1(a)]. In the case of open boundary conditions, we set $B_1 = 1$ at the left edge and $B_2 = N$ at the right edge or, as an alternative, B_1 and B_2 close to the edges [see Figs. 1(b) and 1(c)]. This alternative will be discussed in detail later. For all choices of B_1 and B_2 , the first (second) bath induces a net polarization of order μ ($-\mu$), leading to a steady state in the long-time limit with a characteristic density profile and a constant current.

In this open scenario, we are interested in the dynamics of local magnetization, occurring at finite times and in the long-time limit. Thus, we study expectation values

$$\langle S_r^z(t) \rangle = \text{tr}[\rho(t) S_r^z], \quad (19)$$

which depends on the parameters of the Hamiltonian H and also on the two bath parameters μ and γ . As the initial condition, we choose $\rho(0) \propto 1$, which corresponds to the high-temperature limit $\beta \rightarrow 0$ and a homogeneous profile of magnetization.

V. STOCHASTIC UNRAVELING OF THE LINDBLAD EQUATION

We aim to find a solution of the Lindblad equation or an accurate approximation of the same. To this end, we rely on

the concept of stochastic unraveling, which uses pure states $|\psi\rangle$ rather than density matrices ρ [56,57]. This concept consists of an alternating sequence of stochastic jumps with one of the Lindblad operators and, between the stochastic jumps, a deterministic time evolution with respect to an effective Hamiltonian,

$$H_{\text{eff}} = H - \frac{i}{2} \sum_j \alpha_j L_j^\dagger L_j. \quad (20)$$

For our choice of Lindblad operators in Eqs. (15)–(18), this effective Hamiltonian takes on the form

$$H_{\text{eff}} = H - i\gamma + i\gamma\mu(n_{B_1} - n_{B_2}), \quad (21)$$

with the occupation number $n_r = S_r^+ S_r^- = S_r^z + 1/2$. In this work, we focus on the weak-driving case. For $\mu \ll 1$, H_{eff} can be approximated as

$$H_{\text{eff}} \approx H - i\gamma. \quad (22)$$

Hence, the time evolution with respect to H_{eff} becomes

$$|\psi(t)\rangle \approx e^{-\gamma t} e^{-iHt} |\psi\rangle. \quad (23)$$

Therefore, the dynamics of a pure state is generated by only the closed system H , apart from the scalar damping term. This fact will be one of the main ingredients to connect the closed system and the weakly driven open system. For larger μ , the dynamics is more complicated and also involves the operators n_{B_1} and n_{B_2} .

Since H_{eff} is non-Hermitian, the norm of the pure state $\psi(t)$ is not conserved and decays over the course of time [see Eq. (23)]. Therefore, at some time $t = \tau$, the condition $\|\psi(t)\|^2 > \varepsilon$ is first violated for a given ε , which is here drawn at random from a box distribution $[0,1]$. At this point in time, a stochastic jump with one of the Lindblad operators takes place. The new and normalized pure state reads [57]

$$|\psi'(t)\rangle = \frac{L_j |\psi(t)\rangle}{\|L_j |\psi(t)\rangle\|}, \quad (24)$$

where the specific jump is chosen with probability

$$p_j = \frac{\alpha_j \|L_j |\psi(t)\rangle\|^2}{\sum_{j=1}^4 \alpha_j \|L_j |\psi(t)\rangle\|^2}. \quad (25)$$

After the jump, the procedure continues with the next deterministic time evolution with respect to H_{eff} .

This sequence of stochastic jumps and deterministic evolutions leads to a particular trajectory $|\psi_T(t)\rangle$. The time-dependent density matrix according to the Lindblad equation can eventually be approximated by the average over different trajectories T . Thus, the expectation value reads

$$\langle S_r^z(t) \rangle \approx \frac{1}{T_{\text{max}}} \sum_{T=1}^{T_{\text{max}}} \frac{\langle \psi_T(t) | S_r^z | \psi_T(t) \rangle}{\|\psi_T(t)\|^2}, \quad (26)$$

where T_{max} is a large enough number of trajectories. For $T_{\text{max}} \rightarrow \infty$, the approximation becomes an equality, and the stochastic unraveling can be used as an, in principle, exact numerical technique. Moreover, it will provide the basis for an analytical connection between closed-system and open-system dynamics.

As already mentioned above, we consider $\rho(0) \propto 1$ to be the initial condition of the Lindblad equation, which is realized in the stochastic unraveling via a random pure state $|\psi(0)\rangle$ of the form in Eq. (8).

VI. CONNECTION BETWEEN CLOSED AND OPEN SYSTEMS

A. Time evolution

Now, we are ready to discuss our central prediction, which specifically connects the dynamics in closed and open systems. While this prediction was presented in our previous work [52,58] in detail, we repeat here parts of the derivation which will be of help in understanding the results presented afterwards.

The derivation is based on the stochastic unraveling of the Lindblad equation. It is important to recall that we focus on the weak-driving case $\mu \ll 1$. In this case, the deterministic evolution with respect to H_{eff} is unitary apart from a scalar damping term [see Eq. (23)]. As a consequence, when we calculate the quantity

$$d_r(t) = \frac{\langle \psi_T(t) | S_r^z | \psi_T(t) \rangle}{\| |\psi_T(t)\rangle \|^2}, \quad (27)$$

this scalar cancels out. Because the initial condition is a random state of the form in Eq. (8), the first deterministic evolution is quite simple. Under unitary time evolution, a random state remains a random state with a uniform density profile, $d_r(t) = 0$. Therefore, the first nontrivial event is the subsequent jump.

Without loss of generality, let us consider at some time $t = \tau$ a specific jump with one of the Lindblad operators, e.g., L_1 . Then, the resulting pure state reads

$$|\psi'(\tau)\rangle \propto L_1 |\psi(\tau - 0^+)\rangle, \quad (28)$$

which has exactly the same structure as the pure state in Eq. (11). Hence, we can employ dynamical quantum typicality and get

$$\frac{d_r(t)}{2} \approx \Theta(t - \tau) \langle S_r^z(t - \tau) S_{B_1}^z(0) \rangle_{\text{eq}}, \quad (29)$$

where $\Theta(t)$ is the Heaviside function. Using the same arguments, we can obtain analogous relations for the remaining Lindblad operators L_j , which then involve either $\langle S_r^z(t) S_{B_1}^z(0) \rangle_{\text{eq}}$ or $\langle S_r^z(t) S_{B_2}^z(0) \rangle_{\text{eq}}$. Afterwards, averaging over all four jump possibilities yields

$$\begin{aligned} \frac{\bar{d}_r(t)}{2} &\approx (p_1 - p_2) \Theta(t - \tau) \langle S_r^z(t - \tau) S_{B_1}^z(0) \rangle_{\text{eq}} \\ &+ (p_3 - p_4) \Theta(t - \tau) \langle S_r^z(t - \tau) S_{B_2}^z(0) \rangle_{\text{eq}}, \end{aligned} \quad (30)$$

with jump probabilities $p_j = \alpha_j/4\gamma$ for a random state [see Eq. (25)]. Finally, by inserting the prefactors α_j from Eqs. (15)–(18), we end up with

$$\begin{aligned} \bar{d}_r(t) &\approx \mu \Theta(t - \tau) \langle S_r^z(t - \tau) S_{B_1}^z(0) \rangle_{\text{eq}} \\ &- \mu \Theta(t - \tau) \langle S_r^z(t - \tau) S_{B_2}^z(0) \rangle_{\text{eq}} \end{aligned} \quad (31)$$

for the expectation value after the first jump.

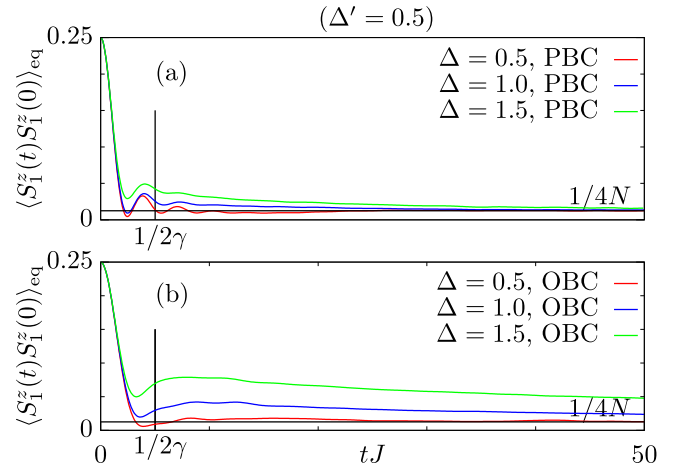


FIG. 3. Temporal decay of the autocorrelation function $\langle S_I^z(t) S_I^z(0) \rangle_{\text{eq}}$ for (a) periodic boundary conditions and (b) open boundary conditions, as obtained numerically for the Hamiltonian H' in Eq. (3) for different Δ at fixed $\Delta' = 0.5$ and $N = 20$. The equilibration value $1/(4N)$ and the timescale $1/(2\gamma)$, with $\gamma/J = 0.1$, are indicated.

To proceed, a natural idea is to reuse the same line of reasoning for the second and all subsequent jumps. After the first jump, however, the pure state is different since it has an inhomogeneous density profile with magnetization concentrated at the site of the bath contact. Thus, one has to wait until the injected magnetization has spread over a piece of the system. Clearly, such a waiting time requires a small enough value of the system-bath coupling γ , as illustrated in Fig. 3. This kind of equilibration is a central ingredient, and its impact will be scrutinized for specific models later. Assuming equilibration, we can iterate the arguments and obtain a superposition of the form

$$\begin{aligned} \frac{\bar{d}_r(t)}{2\mu} &\approx \sum_j A_j \Theta(t - \tau_j) [\langle S_r^z(t - \tau_j) S_{B_1}^z(0) \rangle_{\text{eq}} \\ &- \langle S_r^z(t - \tau_j) S_{B_2}^z(0) \rangle_{\text{eq}}], \end{aligned} \quad (32)$$

where the amplitudes A_j can be calculated from the jump probabilities in Eq. (25) and result in [52]

$$A_j = \frac{a_j - \bar{d}_{B_1}(\tau_j - 0^+)}{\mu}, \quad (33)$$

with

$$a_j = \frac{\mu - 2\bar{d}_{B_1}(\tau_j - 0^+)}{2 - 4\mu\bar{d}_{B_1}(\tau_j - 0^+)}. \quad (34)$$

If $\bar{d}_{B_1}(\tau_j - 0^+) \rightarrow 0$, $A_j \rightarrow 1/2$.

Because the expression in Eq. (32) applies to a single sequence of jump times, (τ_1, τ_2, \dots) , the final prediction is obtained with the average

$$\langle S_r^z(t) \rangle \approx \frac{1}{T_{\text{max}}} \sum_{T=1}^{T_{\text{max}}} \bar{d}_{r,T}(t) \quad (35)$$

over trajectories with different jump times. Due to the scalar damping term in Eq. (23), these jump times are given by

$$\tau_{j+1} = \tau_j - \ln \frac{\varepsilon_{j+1}}{2\gamma}, \quad (36)$$

where ε_{j+1} is drawn at random from a box distribution $[0,1]$ again.

In principle, the prediction in Eqs. (32) and (35) can be calculated analytically for a specific model. However, the closed-system correlation functions $\langle S_r^z(t) S_{B_1}^z(0) \rangle_{\text{eq}}$ and $\langle S_r^z(t) S_{B_2}^z(0) \rangle_{\text{eq}}$ are often available only numerically, such that the prediction has to be calculated numerically as well.

B. Injected magnetization

While Eqs. (32) and (35) allow us to predict the dynamics of magnetization at finite times and in the limit of long times, a similar expression can be derived for the respective currents in the steady state. To this end, let us consider the magnetization injected by the first bath, which can be predicted as [52]

$$\langle \delta S_{B_1}^z(t) \rangle \approx \frac{1}{T_{\text{max}}} \sum_{T=1}^{T_{\text{max}}} \delta \bar{d}_{B_1,T}(t), \quad (37)$$

with δ being just a notation for “injected” and

$$\frac{\delta \bar{d}_{B_1,T}(t)}{2\mu} \approx \sum_j A_j \Theta(t - \tau_j) \langle [S_{B_1}^z(0)]^2 \rangle, \quad (38)$$

which is slightly simpler than Eq. (32). Since in the steady state all currents are the same,

$$\langle j_r \rangle = \langle j_{r'} \rangle, \quad B_1 \leq r, \quad r' \leq B_2, \quad (39)$$

it is sufficient to know $\langle j_{B_1} \rangle$, which can be expressed as

$$\langle j_{B_1} \rangle = \frac{d}{dt} \frac{\langle \delta S_{B_1}^z(t) \rangle}{f}. \quad (40)$$

Here, $f = 2$ for periodic boundary conditions (flow to the right and left of the bath), and $f = 1$ for open boundary conditions (flow only to the right of the bath).

With knowledge of the steady-state current, it is also possible to predict the diffusion constant via [20]

$$D = - \frac{\langle j_r \rangle}{\langle S_{r+1}^z \rangle - \langle S_r^z \rangle} \quad (41)$$

for some site r in the bulk.

VII. RESULTS

A. Next-nearest-neighbor interactions and periodic boundary conditions

Finally, we turn to our numerical simulations, in which the central goal is to analyze the quality of the prediction in Eqs. (32) and (35) for various situations. To start with, we investigate the spin-1/2 XXZ chain with interactions between next-nearest neighbors, Eq. (3), and the case of periodic boundary conditions [Fig. 1(a)]. Afterwards, we additionally study other perturbations and the case of open boundary conditions with different bath-coupling geometries.

Because a main ingredient of the prediction has been the equilibration of the injected magnetization, we first focus

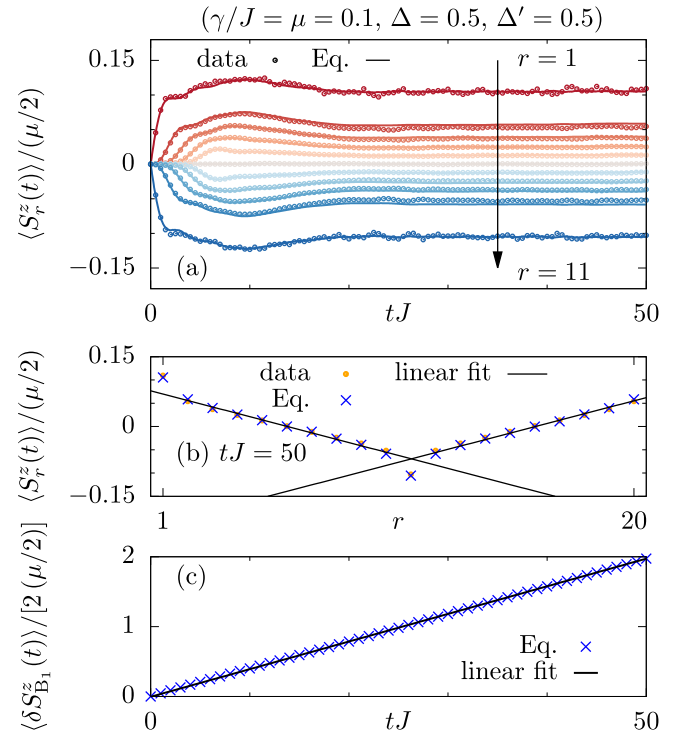


FIG. 4. Open-system dynamics for the model H' in Eq. (3), as obtained numerically for $\Delta = 0.5$, $\Delta' = 0.5$, $N = 20$, periodic boundary conditions, small coupling $\gamma/J = 0.1$, and weak driving $\mu = 0.1$. Exact results from the full stochastic unraveling (data) are compared to the prediction (labeled “Eq.”), which is based on spatio-temporal correlation functions in the closed system. (a) Time evolution of the local magnetization $\langle S_r^z(t) \rangle$ for different sites r . (b) Site dependence of the steady state at $tJ = 50$. (c) Magnetization injected by the first bath as a function of time.

on this assumption. To this end, we numerically calculate in Fig. 3(a) the equal-site correlation function $\langle S_r^z(t) S_r^z(0) \rangle_{\text{eq}}$ for $\Delta' = 0.5$, $N = 20$, and an arbitrary site r due to periodic boundary conditions. Apparently, for all Δ depicted, this function starts with the initial value $1/4$, decays substantially on a timescale $t_R J \approx 5$, and then approaches the equilibration value $1/(4N)$ in the limit of long times. By comparing t_R to $1/(2\gamma)$ from Eq. (36), we identify $\gamma/J = 0.1$ as a reasonable choice for the system-bath coupling, which we fix from now on for a fair comparison, together with the choice $\mu = 0.1$ to ensure weak driving.

For the value $\Delta = 0.5$, we depict in Fig. 4(a) the time evolution of magnetization in the open system. Here, the prediction is carried out for $\approx 10\,000$ different sequences of jump times, which already yields smooth curves. The full stochastic unraveling, without any assumption, was evaluated on clusters and turns out to require as many as $\approx 200\,000$ (or more) sequences for a comparable smoothness [59]. Despite residual statistical fluctuations, the agreement is almost perfect and is clearly visible from short to long times. This convincing agreement can also be seen for the steady-state profile in Fig. 4(b). Compared to previous results for integrable systems [52], the degree of agreement turns out to be similar. This finding indicates that nonintegrability is not required for the

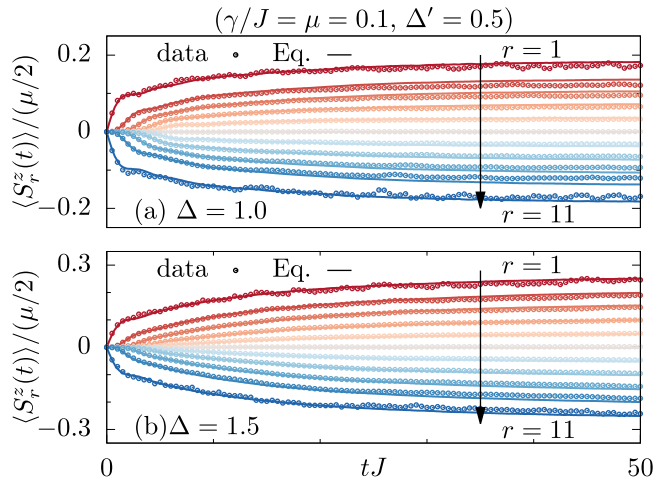


FIG. 5. Similar data to those in Fig. 4(a), but now for (a) $\Delta = 1.0$ and (b) $\Delta = 1.5$.

prediction to hold, which is consistent with the fact that such an assumption does not enter the derivation.

In Fig. 4(c), we also show the injected magnetization, which grows linearly with time. From the slope and the slope of the steady-state density profile in Fig. 4(b), we can extract a diffusion constant via Eq. (41). The value $D/J \approx 2.9$ agrees well with other values in the literature, such as $D/J \approx 3.1$ in the closed system [60,61], and serves as a further reality check of our approach.

To ensure that our results do not depend on the specific choice of parameters, we redo in Fig. 5 the calculation for other $\Delta \neq 0.5$. The overall agreement is apparently the same.

B. Open boundary conditions and different bath-coupling geometries

Now, we move forward to the case of open boundary conditions with a standard bath coupling at the edges, as sketched in Fig. 1(b). For such a situation, it is also possible to obtain the solution of the Lindblad equation using TEBD [19,62] as a state-of-the-art technique in this context. For the same Hamiltonian and parameters as before, we depict in Fig. 6 the numerical result from TEBD and additionally make a comparison to the exact stochastic-unraveling procedure. Even though statistical fluctuations are again visible, both approaches coincide for all times and Δ depicted. This agreement particularly confirms the correctness of our numerics.

When we compare TEBD to the actual prediction in Fig. 7, the agreement is less convincing for long times and becomes worse for larger values of Δ . To understand the origin of the disagreement, we test the assumption of equilibration by calculating in Fig. 3(b) the equal-site correlation function $\langle S_r^z(t)S_r^z(0) \rangle_{\text{eq}}$ at the left-edge site $r = 1$. In contrast to periodic boundary conditions, this function decays slower and develops long-time tails for large Δ , which can be traced back to nondecaying edge modes occurring for $\Delta > 1$ [63,64]. As the occurrence of long-time tails in Fig. 3(b) seems to correlate with the degree of disagreement in Fig. 7, we can identify the breakdown of the assumption as the origin.

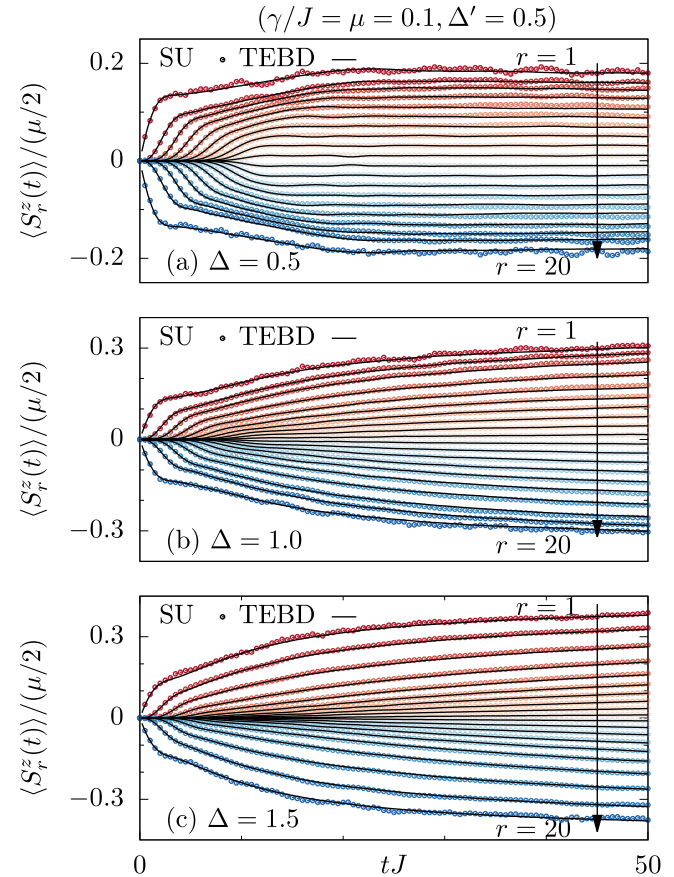


FIG. 6. Comparison of the solution of the Lindblad equation, as obtained numerically from stochastic unraveling (SU) and time-evolving block decimation (TEBD), for the Hamiltonian H' in Eq. (3) with (a) $\Delta = 0.5$, (b) $\Delta = 1.0$, and (c) $\Delta = 1.5$ as well as $N = 20$, open boundary conditions, $\gamma/J = 0.1$, and $\mu = 0.1$.

For $\Delta = 0.5$, where the assumption is fulfilled best, we next increase the system size to $N = 34 \gg 20$. For such a system size, the Hilbert-space dimension becomes huge, and stochastic unraveling is no longer feasible due to the many trajectories required. However, the prediction can still be carried out since the two correlation functions $\langle S_r^z(t)S_{B_1}^z(0) \rangle_{\text{eq}}$ and $\langle S_r^z(t)S_{B_2}^z(0) \rangle_{\text{eq}}$ need to be calculated only once. In particular, this calculation is possible with the use of dynamical quantum typicality and supercomputers. In Fig. 8, we depict the corresponding prediction and make a comparison to the TEBD solution, which up to times $tJ \approx 50$ does not depend on the bond dimension used. (A convergence analysis of TEBD can be found in Appendix A.) The convincing agreement supports the idea that our prediction is a useful alternative for large system sizes, which are usually accessible by only matrix-product states.

Unfortunately, our assumption is not always satisfied for open boundary conditions, as discussed above. Hence, we explore possibilities to circumvent this problem. To this end, we consider the slightly different bath-coupling geometry in Fig. 1(c), where the Lindblad operators are not located exactly at the edges, but close to them. As depicted in Fig. 9(a), the equal-site correlation function $\langle S_r^z(t)S_r^z(0) \rangle_{\text{eq}}$ tends to decay more strongly when the site r is moved away from the left

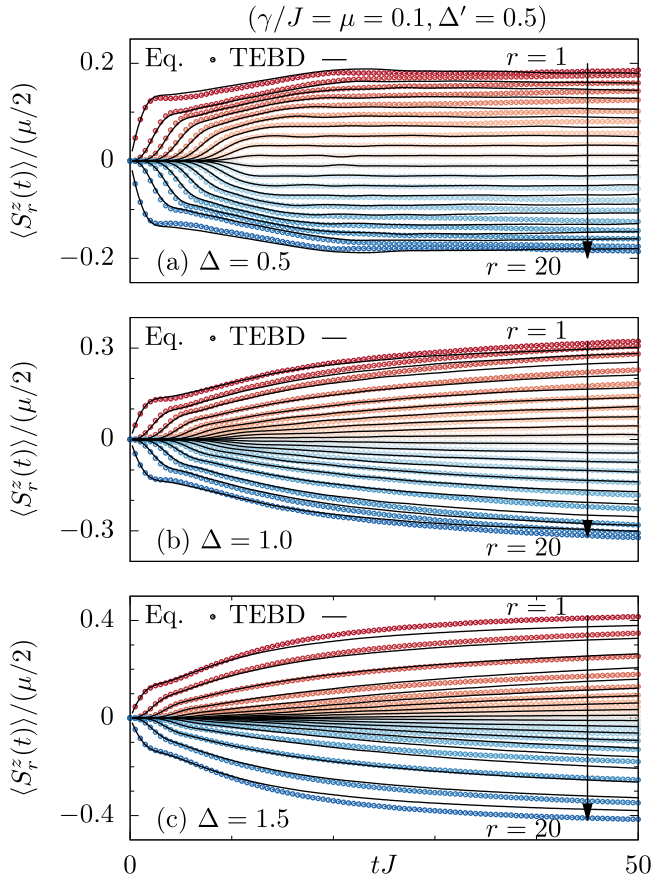


FIG. 7. The same as Fig. 6, but instead of stochastic unraveling, a comparison between the prediction (labeled “Eq.,”) and time-evolving block decimation (TEBD).

edge $r = 1$, indicating a higher degree of equilibration. Indeed, for the so far worst case $\Delta = 1.5$, the prediction for the open-system dynamics in Fig. 9(b) agrees substantially better with the full stochastic unraveling. This observation supports the usefulness of other bath-coupling geometries which have attracted less attention so far.

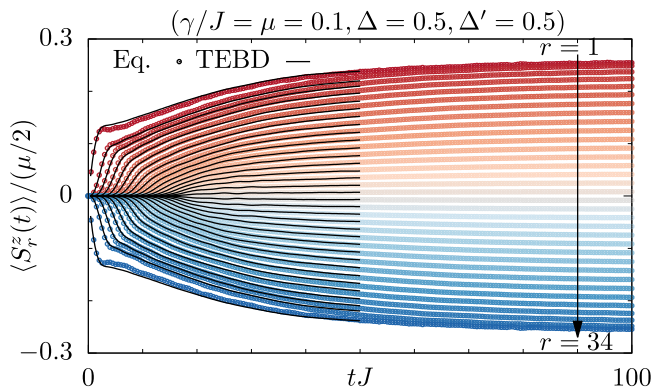


FIG. 8. The same as Fig. 7(a), but now for system size $N = 34 \gg 20$, where stochastic unraveling is no longer possible.

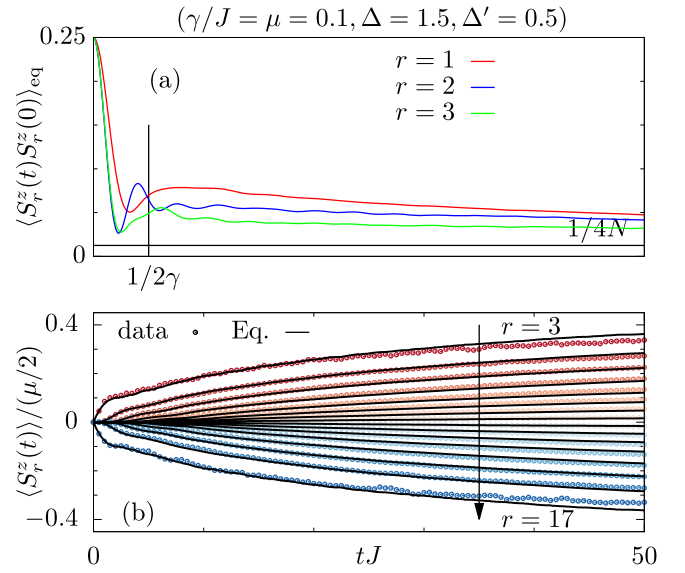


FIG. 9. Bath coupling close to the edges. (a) Temporal decay of the autocorrelation function $\langle S_r^z(t) S_r^z(0) \rangle_{\text{eq}}$ for different sites r , as obtained numerically for the model H' in Eq. (3) with $\Delta = 1.5$, $\Delta' = 0.5$, $N = 20$, and open boundary conditions. (b) Open-system dynamics for bath coupling at sites $B_1 = 3$ and $B_2 = 17$. In comparison to the data in Fig. 7(c), the agreement between the prediction (labeled “Eq.,”) and stochastic unraveling (“data”) is better.

C. Staggered field

Finally, we also study other perturbations and turn to the spin-1/2 XXZ chain with a staggered field, Eq. (4), where we focus on $\Delta = 1.0$, $B/J = 0.5$, and $N = 20$. In Fig. 10, we summarize our numerical results. Apparently, the situation is overall similar. The equal-site correlation function $\langle S_r^z(t) S_r^z(0) \rangle_{\text{eq}}$ in Fig. 10(a) behaves differently for periodic and open boundary conditions. Consistently, the prediction for the open-system dynamics agrees well with numerics for the periodic boundary case in Fig. 10(b), while deviations are visible for the open boundary case in Fig. 10(c). We have checked that the situation remains the same for other parameters of Δ , although that is not explicitly shown here.

VIII. CONCLUSION

To summarize, we studied the Lindblad equation as a central approach to boundary-driven magnetization transport in spin-1/2 chains. Our main motivation was to understand to what extent the dynamics in the open system, at finite times and in the limit of long times, can be predicted on the basis of the dynamics in a closed system. To that end, we followed the idea of a previous work [52] which suggested prediction in terms of spatio-temporal correlation functions, Eqs. (32) and (35), given the case of weak driving and small system-bath coupling. While that work focused on integrable systems and periodic boundary conditions, we substantially extended the analysis in the current work by going in three different directions: (1) We considered nonintegrable systems, (2) we included open boundary conditions and other bath-coupling geometries, and (3) we provided a comparison with time-evolving block decimation.

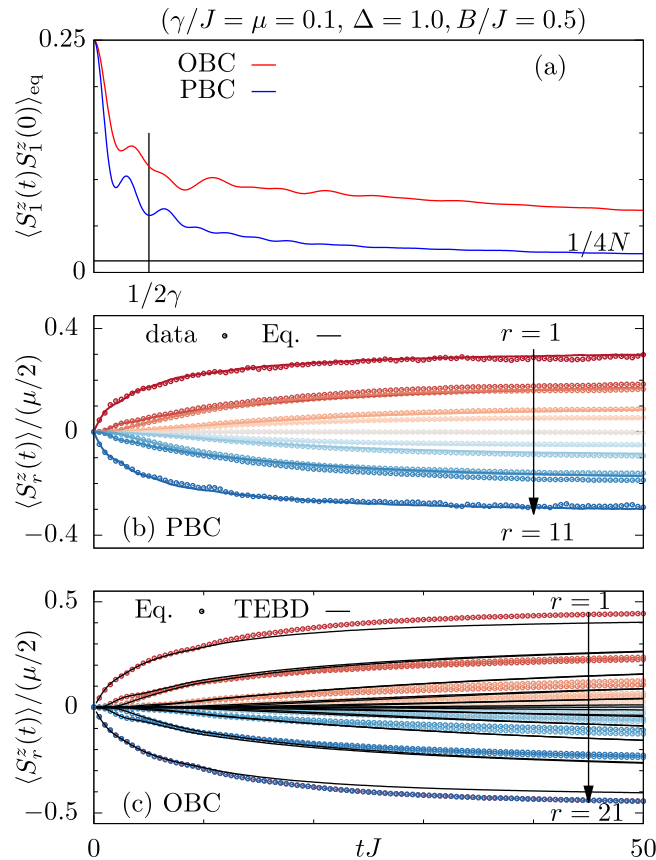


FIG. 10. Another model: staggered field. (a) Temporal decay of the autocorrelation function $\langle S_1^z(t)S_1^z(0) \rangle_{\text{eq}}$ for closed and open boundary conditions, as obtained numerically for the Hamiltonian H'' in Eq. (4) with $\Delta = 1.0$, $B/J = 0.5$, and $N = 20$. (b) and (c) Open-system dynamics for the respective boundary conditions as well as $\gamma/J = 0.1$ and $\mu = 0.1$. The prediction (labeled “Eq.”) is compared to either stochastic unraveling (“data”) or time-evolving block decimation (TEBD).

We found that nonintegrability plays a minor role since the quality of the prediction is comparable to the one for integrable systems. This observation is consistent with the fact that nonintegrability does not enter as an assumption in the derivation. In contrast, the choice of the specific boundary conditions has turned out to be relevant. For periodic boundary conditions, on the one hand, prediction and numerical simulations agreed convincingly for all models and parameters considered here. For open boundary conditions, on the other hand, we observed some disagreement in particular cases, which we traced back to slowly decaying edge modes and thus a breakdown of the equilibration assumption underlying the prediction. In this context, it is important to note that the validity of the assumption can be checked in advance and does not require a comparison to other methods. To circumvent such edge modes, we also explored other bath-coupling geometries, in which the Lindblad operators do not act exactly at the boundary sites, but close to them.

For parameters for which the assumption is well fulfilled also for open boundary conditions, we demonstrated that the prediction yields an accurate description and can be carried out for comparatively large system sizes, which are usually

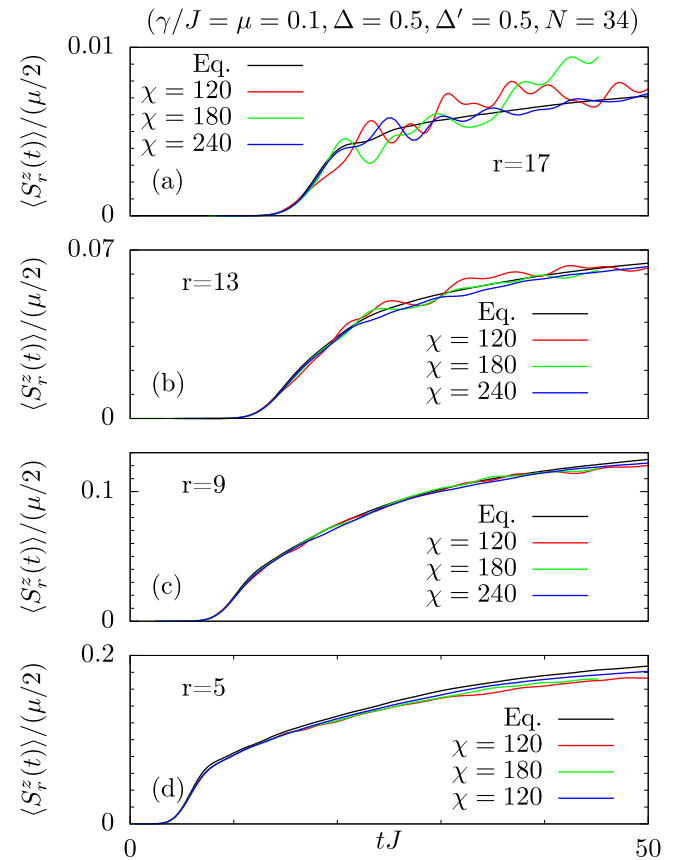


FIG. 11. Convergence analysis. The data in Fig. 8 are depicted again for different sites: (a) $r = 17$, (b) $r = 13$, (c) $r = 9$, and (d) $r = 5$. But now, the prediction (labeled “Eq.”) is compared to data from time-evolving block decimation (TEBD) for various bond dimensions χ . While $r = 5$ is close to the edge, $r = 17$ lies in the bulk.

accessible by only matrix-product-state methods. From a less practical but more physical perspective, we have thus shown a kind of one-to-one correspondence between the time evolution in open and closed systems, at least for the models considered by us.

Promising directions for future research include quasi-one-dimensional lattices, finite temperatures, energy transport, fermionic models, and disorder. Another interesting avenue would be to explore in which cases the slowly decaying edge modes of the closed system can be enhanced in an open system [65].

ACKNOWLEDGMENTS

Our work was funded by the Deutsche Forschungsgemeinschaft (DFG), Projects No. 397107022 (GE 1657/3-2), No. 397300368 (MI 1772/4-2), and No. 397067869 (STE 2243/3-2), within DFG Research Unit FOR 2692, Grant No. 355031190. J.R. acknowledges funding from the European Union’s Horizon Europe research and innovation program, Marie Skłodowska-Curie Grant No. 101060162, and the Packard Foundation through a Packard Fellowship in Science and Engineering. We gratefully acknowledge the Gauss Centre for Supercomputing e. V. for funding this project

by providing computing time on the GCS Supercomputer JUWELS6 at the Jülich Supercomputing Centre (JSC). S.N. was supported by QuantERA grants QuSiED and T-NiSQ, by MVZI, QuantERA II JTC 2021. TEBD calculations were performed on the supercomputer Vega at the Institute of Information Science (IZUM) in Maribor, Slovenia.

APPENDIX A: CONVERGENCE OF THE TEBD METHOD

In the main text, we showed in Fig. 8 numerical data from TEBD and stated that, up to times $tJ \approx 50$, it does not depend on the bond dimension χ used. To further substantiate this statement, we depict in Fig. 11 the same data for different χ and various sites, close to the edges and in the bulk. While the data are particularly well converged close to the edges, some oscillations can be seen in the bulk, where the time evolution is kind of close to unitary.

APPENDIX B: CORRELATION FUNCTIONS FOR OPEN BOUNDARY CONDITIONS

In Fig. 3(b), we show the equal-site correlation function $\langle S_r^z(t)S_r^z(0) \rangle_{\text{eq}}$ for the open boundary case and different Δ , where we focus on a single system size, $N = 20$. To demonstrate that the temporal decay does not depend significantly on system size, we additionally depict in Fig. 12(a) numerical data for $N = 24$. For completeness, Fig. 12(b) shows

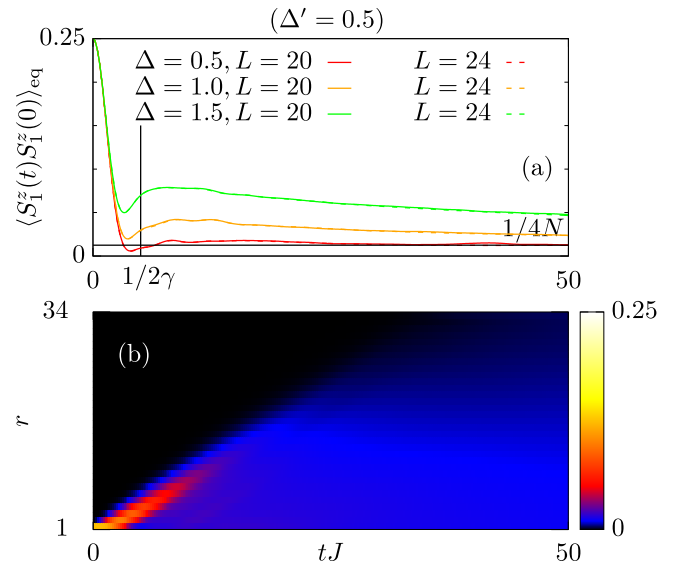


FIG. 12. (a) Dynamics of the autocorrelation function $\langle S_1^z(t)S_1^z(0) \rangle_{\text{eq}}$ for open boundary conditions, as depicted in Fig. 3(b) for different Δ , but now for two system sizes, $N = 20$ and $N = 24$. (b) Time-space density plot of the correlation functions $\langle S_r^z(t)S_r^z(0) \rangle_{\text{eq}}$ for $N = 34$ and $\Delta = 0.5$, which are used for the prediction in Fig. 8.

the full time-space dependence of the correlation functions $\langle S_r^z(t)S_r^z(0) \rangle_{\text{eq}}$ for $N = 34$ and $\Delta = 0.5$, which were used for the prediction in Fig. 8.

- [1] I. Bloch, J. Dalibard, and W. Zwerger, Many-body physics with ultracold gases, *Rev. Mod. Phys.* **80**, 885 (2008).
- [2] D. A. Abanin, E. Altman, I. Bloch, and M. Serbyn, *Colloquium: Many-body localization, thermalization, and entanglement*, *Rev. Mod. Phys.* **91**, 021001 (2019).
- [3] A. Polkovnikov, K. Sengupta, A. Silva, and M. Vengalattore, *Colloquium: Nonequilibrium dynamics of closed interacting quantum systems*, *Rev. Mod. Phys.* **83**, 863 (2011).
- [4] J. Eisert, M. Friesdorf, and C. Gogolin, Quantum many-body systems out of equilibrium, *Nat. Phys.* **11**, 124 (2015).
- [5] L. D'Alessio, Y. Kafri, A. Polkovnikov, and M. Rigol, From quantum chaos and eigenstate thermalization to statistical mechanics and thermodynamics, *Adv. Phys.* **65**, 239 (2016).
- [6] J. M. Deutsch, Quantum statistical mechanics in a closed system, *Phys. Rev. A* **43**, 2046 (1991).
- [7] M. Srednicki, Chaos and quantum thermalization, *Phys. Rev. E* **50**, 888 (1994).
- [8] M. Rigol, V. Dunjko, and M. Olshanii, Thermalization and its mechanism for generic isolated quantum systems, *Nature (London)* **452**, 854 (2008).
- [9] C. Bartsch and J. Gemmer, Dynamical typicality of quantum expectation values, *Phys. Rev. Lett.* **102**, 110403 (2009).
- [10] J. Gemmer, M. Michel, and G. Mahler, *Quantum Thermodynamics*, Lecture Notes in Physics Vol. 657 (Springer, Berlin, 2004).
- [11] S. Goldstein, J. L. Lebowitz, R. Tumulka, and N. Zanghi, Canonical typicality, *Phys. Rev. Lett.* **96**, 050403 (2006).
- [12] S. Popescu, A. J. Short, and A. Winter, Entanglement and the foundations of statistical mechanics, *Nat. Phys.* **2**, 754 (2006).
- [13] P. Reimann, Typicality for generalized microcanonical ensembles, *Phys. Rev. Lett.* **99**, 160404 (2007).
- [14] T. A. Elsayed and B. V. Fine, Regression relation for pure quantum states and its implications for efficient computing, *Phys. Rev. Lett.* **110**, 070404 (2013).
- [15] R. Steinigeweg, J. Gemmer, and W. Brenig, Spin-current auto-correlations from single pure-state propagation, *Phys. Rev. Lett.* **112**, 120601 (2014).
- [16] T. Heitmann, J. Richter, D. Schubert, and R. Steinigeweg, Selected applications of typicality to real-time dynamics of quantum many-body systems, *Z. Naturforsch. A* **75**, 421 (2020).
- [17] F. Jin, D. Willsch, M. Willsch, H. Lagemann, K. Michielsen, and H. De Raedt, Random state technology, *J. Phys. Soc. Jpn.* **90**, 012001 (2021).
- [18] U. Schollwöck, The density-matrix renormalization group, *Rev. Mod. Phys.* **77**, 259 (2005).
- [19] U. Schollwöck, The density-matrix renormalization group in the age of matrix product states, *Ann. Phys. (NY)* **326**, 96 (2011).
- [20] B. Bertini, F. Heidrich-Meisner, C. Karrasch, T. Prosen, R. Steinigeweg, and M. Žnidarič, Finite-temperature transport in one-dimensional quantum lattice models, *Rev. Mod. Phys.* **93**, 025003 (2021).

- [21] R. Kubo, M. Toda, and N. Hashisume, *Statistical Physics II: Nonequilibrium Statistical Mechanics*, Springer Series in Solid-State Sciences Vol. 31 (Springer, Berlin, 1991).
- [22] A. Bastianello, B. Bertini, B. Doyon, and R. Vasseur, Introduction to the special issue on emergent hydrodynamics in integrable many-body systems, *J. Stat. Mech.* (2022) 014001.
- [23] B. Doyon, S. Gopalakrishnan, F. Møller, J. Schmiedmayer, and R. Vasseur, Generalized hydrodynamics: A perspective, [arXiv:2311.03438](https://arxiv.org/abs/2311.03438).
- [24] T. Prosen and M. Žnidarič, Matrix product simulations of non-equilibrium steady states of quantum spin chains, *J. Stat. Mech.* (2009) P02035.
- [25] M. Michel, M. Hartmann, J. Gemmer, and G. Mahler, Fourier's law confirmed for a class of small quantum systems, *Eur. Phys. J. B* **34**, 325 (2003).
- [26] H. Wichterich, M. J. Henrich, H.-P. Breuer, J. Gemmer, and M. Michel, Modeling heat transport through completely positive maps, *Phys. Rev. E* **76**, 031115 (2007).
- [27] M. Žnidarič, Spin transport in a one-dimensional anisotropic Heisenberg model, *Phys. Rev. Lett.* **106**, 220601 (2011).
- [28] H.-P. Breuer and F. Petruccione, *The Theory of Open Quantum Systems* (Oxford University Press, Oxford, 2007).
- [29] H. De Raedt, F. Jin, M. I. Katsnelson, and K. Michielsen, Relaxation, thermalization, and Markovian dynamics of two spins coupled to a spin bath, *Phys. Rev. E* **96**, 053306 (2017).
- [30] F. Verstraete, J. J. García-Ripoll, and J. I. Cirac, Matrix product density operators: Simulation of finite-temperature and dissipative systems, *Phys. Rev. Lett.* **93**, 207204 (2004).
- [31] M. Zwolak and G. Vidal, Mixed-state dynamics in one-dimensional quantum lattice systems: A time-dependent super-operator renormalization algorithm, *Phys. Rev. Lett.* **93**, 207205 (2004).
- [32] H. Weimer, A. Kshetrimayum, and R. Orús, Simulation methods for open quantum many-body systems, *Rev. Mod. Phys.* **93**, 015008 (2021).
- [33] T. Prosen, Open XXZ spin chain: Nonequilibrium steady state and a strict bound on ballistic transport, *Phys. Rev. Lett.* **106**, 217206 (2011).
- [34] T. Prosen and E. Ilievski, Families of quasilocal conservation laws and quantum spin transport, *Phys. Rev. Lett.* **111**, 057203 (2013).
- [35] M. Ljubotina, M. Žnidarič, and T. Prosen, Kardar-Parisi-Zhang physics in the quantum Heisenberg magnet, *Phys. Rev. Lett.* **122**, 210602 (2019).
- [36] S. Gopalakrishnan and R. Vasseur, Kinetic theory of spin diffusion and superdiffusion in XXZ spin chains, *Phys. Rev. Lett.* **122**, 127202 (2019).
- [37] V. B. Bulchandani, S. Gopalakrishnan, and E. Ilievski, Superdiffusion in spin chains, *J. Stat. Mech.* (2021) 084001.
- [38] S. Nandy, Z. Lenarčič, E. Ilievski, M. Mierzejewski, J. Herbrych, and P. Prelovšek, Spin diffusion in a perturbed isotropic Heisenberg spin chain, *Phys. Rev. B* **108**, L081115 (2023).
- [39] M. Serbyn, D. A. Abanin, and Z. Papić, Quantum many-body scars and weak breaking of ergodicity, *Nat. Phys.* **17**, 675 (2021).
- [40] H. Singh, B. A. Ware, R. Vasseur, and A. J. Friedman, Subdiffusion and many-body quantum chaos with kinetic constraints, *Phys. Rev. Lett.* **127**, 230602 (2021).
- [41] J. Richter and A. Pal, Anomalous hydrodynamics in a class of scarred frustration-free Hamiltonians, *Phys. Rev. Res.* **4**, L012003 (2022).
- [42] J. Richter, O. Lunt, and A. Pal, Transport and entanglement growth in long-range random Clifford circuits, *Phys. Rev. Res.* **5**, L012031 (2023).
- [43] R. M. Nandkishore and D. A. Huse, Many-body localization and thermalization in quantum statistical mechanics, *Annu. Rev. Condens. Matter Phys.* **6**, 15 (2015).
- [44] D. J. Luitz and Y. B. Lev, The ergodic side of the many-body localization transition, *Ann. Phys.* **529**, 1600350 (2017).
- [45] R. Steinigeweg, M. Ogiewa, and J. Gemmer, Equivalence of transport coefficients in bath-induced and dynamical scenarios, *Europhys. Lett.* **87**, 10002 (2009).
- [46] R. Steinigeweg and J. Gemmer, Density dynamics in translationally invariant spin-1/2 chains at high temperatures: A current-autocorrelation approach, *Phys. Rev. B* **80**, 184402 (2009).
- [47] M. Žnidarič and M. Ljubotina, Interaction instability of localization in quasiperiodic systems, *Proc. Natl. Acad. Sci. USA* **115**, 4595 (2018).
- [48] M. Žnidarič, Nonequilibrium steady-state Kubo formula: Equality of transport coefficients, *Phys. Rev. B* **99**, 035143 (2019).
- [49] A. Kundu, A. Dhar, and O. Narayan, The Green-Kubo formula for heat conduction in open systems, *J. Stat. Mech.* (2009) L03001.
- [50] A. Purkayastha, S. Sanyal, A. Dhar, and M. Kulkarni, Anomalous transport in the Aubry-André-Harper model in isolated and open systems, *Phys. Rev. B* **97**, 174206 (2018).
- [51] A. Purkayastha, Classifying transport behavior via current fluctuations in open quantum systems, *J. Stat. Mech.* (2019) 043101.
- [52] T. Heitmann, J. Richter, F. Jin, S. Nandy, Z. Lenarčič, J. Herbrych, K. Michielsen, H. De Raedt, J. Gemmer, and R. Steinigeweg, Spin-1/2 XXZ chain coupled to two Lindblad baths: Constructing nonequilibrium steady states from equilibrium correlation functions, *Phys. Rev. B* **108**, L201119 (2023).
- [53] R. Steinigeweg, H. Wichterich, and J. Gemmer, Density dynamics from current auto-correlations at finite time- and length-scales, *Europhys. Lett.* **88**, 10004 (2009).
- [54] The integrable case $\Delta' = 0$ is also diffusive for the anisotropy $\Delta = 1.5$ [20].
- [55] R. Steinigeweg, F. Jin, D. Schmidtke, H. De Raedt, K. Michielsen, and J. Gemmer, Real-time broadening of nonequilibrium density profiles and the role of the specific initial-state realization, *Phys. Rev. B* **95**, 035155 (2017).
- [56] J. Dalibard, Y. Castin, and K. Mølmer, Wave-function approach to dissipative processes in quantum optics, *Phys. Rev. Lett.* **68**, 580 (1992).
- [57] M. Michel, O. Hess, H. Wichterich, and J. Gemmer, Transport in open spin chains: A Monte Carlo wave-function approach, *Phys. Rev. B* **77**, 104303 (2008).
- [58] T. Heitmann, J. Richter, J. Herbrych, J. Gemmer, and R. Steinigeweg, Real-time broadening of bath-induced density profiles from closed-system correlation functions, *Phys. Rev. E* **108**, 024102 (2023).
- [59] While evaluating the prediction requires only averaging over jump times, the full stochastic unraveling also involves averaging over jump operators, which is the reason for slower convergence.

- [60] J. Wang, M. H. Lamann, R. Steinigeweg, and J. Gemmer, Diffusion constants from the recursion method, [arXiv:2312.02656](#).
- [61] J. Richter and R. Steinigeweg, Combining dynamical quantum typicality and numerical linked cluster expansions, [Phys. Rev. B **99**, 094419 \(2019\)](#).
- [62] F. Verstraete, V. Murg, and J. I. Cirac, Matrix product states, projected entangled pair states, and variational renormalization group methods for quantum spin systems, [Adv. Phys. **57**, 143 \(2008\)](#).
- [63] P. Fendley, Strong zero modes and eigenstate phase transitions in the XYZ/interacting Majorana chain, [J. Phys. A **49**, 30LT01 \(2016\)](#).
- [64] J. Kemp, N. Y. Yao, C. R. Laumann, and P. Fendley, Long coherence times for edge spins, [J. Stat. Mech. \(2017\) 063105](#).
- [65] L. M. Vasiloiu, F. Carollo, and J. P. Garrahan, Enhancing correlation times for edge spins through dissipation, [Phys. Rev. B **98**, 094308 \(2018\)](#).